Experimental and Theoretical Investigations in Two-Dimensional Transonic Flow

DONALD J. COLLINS* AND JAMES A. KRUPP†
Jet Propulsion Laboratory, Pasadena, Calif.

Experimental and theoretical results are presented from a study of the flow over a family of transonically scaled circular-arc bodies mounted in a solid-wall wind tunnel. Data for Reynolds numbers between 1.2×10^6 and 3.6×10^6 based on chord, are compared with the results of computations based on inviscid theory in order to examine the scaling of inviscid transonic flows in a solid-wall wind tunnel, and to obtain a description of the flow near choking. For those cases for which extensive separation of the model and tunnel boundary layers does not occur, excellent agreement between theory and experiment is demonstrated for the flow in the vicinity of the model, and to a lesser degree for the flow near the opposite tunnel boundary. Some results are presented which illustrate the analogy between choked flow in a solid-wall wind tunnel and unbounded flow at $M_\infty = 1.0$.

Nomenclature

c = model chord
$C_p = \dfrac{p-p_\infty}{\frac{1}{2}\rho_\infty {u_\infty}^2}$ — pressure coefficient
$\bar{C}_p = \dfrac{{M_\infty}^{2/3}}{\delta^{2/3}} C_p$ — transonic scaled pressure coefficient
H = symmetric tunnel height
$K = \dfrac{1-{M_\infty}^2}{{M_\infty}^{4/3}\delta^{2/3}}$ — Spreiter transonic scale parameter
Re = Reynolds number based on chord
$T = (H/c)\delta^{1/3}$ — geometrical transonic tunnel parameter
$\tilde{T} = {M_\infty}^{2/3}T$ — Spreiter scaled transonic tunnel parameter
x, y = physical coordinates in units of chord
$\tilde{y} = {M_\infty}^{2/3}\delta^{1/3}y$ — scaled transverse coordinate
$\delta = t/c$ — model thickness ratio
ϕ = perturbation velocity potential

Superscripts
$*$ = sonic speed

Subscripts
∞ = upstream undisturbed flow
ch = choking
crit = critical value
p = peak value
w = wall value

I. Introduction

THE transonic speed regime is the most difficult regime of aircraft flight in which to accurately predict the performance of an aerodynamic surface. Difficulties arise because at transonic speeds the flowfield contains extensive supersonic regions which are bounded by regions of subsonic flow. The equations which describe the flow in this regime are consequently of changing type, exhibiting adjacent regions of elliptic and hyperbolic character, and having embedded shock waves which must be properly modeled. These properties were recognized in the early computations by Spreiter[1] and by Spreiter and Alksne[2] for the unbounded flow over two-dimensional airfoils having simple geometrical profiles. Following the work by Cole,[3] who proposed a different technique for the solution of the transonic small disturbance equation, Murman and Cole,[4] Krupp,[5] and more recently Murman[6] have succeeded in computing the inviscid transonic flow over a variety of both lifting and nonlifting two-dimensional configurations, and have provided a firm basis for the computation of inviscid flows.

When experiments are performed at transonic speeds, a central question which always arises is that of the relationship between the experiment and flight in a uniform unbounded medium. The early work by Guderley[7] and later by Morioka[8] have provided analytic solutions of the approximate transonic equations for conditions of choked flow over geometrically simple bodies in a solid-wall wind tunnel, and have provided information on the scaling of those results for bodies of arbitrary shape. Later work by Spreiter et al.[9] has extended these results and demonstrated the equivalence between choked flow in a solid-wall tunnel and the unbounded uniform flow at $M_\infty = 1.0$.

The present investigation is a combined experimental and theoretical study of the transonic flow over two-dimensional circular-arc profiles in a solid-wall wind tunnel. This investigation has been conducted in an attempt to understand both the scaling of transonic flows in a solid-wall facility and to understand the influence of the experimental boundary conditions on the flowfield at supercritical Mach numbers, with particular emphasis on the choked flow case. In Sec. IVA, experimental evidence is given to support the ideas of inviscid scaling for affine bodies at transonic speeds, a central idea in the computation of inviscid flows. A description is given in Sec. IVB of the phenomenon of choking of an inviscid transonic flow in a solid-wall wind tunnel by examining the results of both theory and experiment. The relationships between choked flow and the unbounded flow at $M_\infty = 1.0$ are discussed, and an extension is suggested to compensate for wall interference at lower Mach numbers. Comparisons between theory and experiment are given in Sec. IVC for the flow over a 6% thick biconvex circular-arc airfoil at a Reynolds number of 1.2×10^6, and the data is compared with that of Knechtel[10] taken under similar conditions in a porous wall transonic tunnel.

Presented as Paper 73-659 at the AIAA 6th Fluid and Plasma Dynamics Conference, Palm Springs, Calif., July 16–18, 1973; submitted July 26, 1973; revision received December 5, 1973. This paper represents the results of one phase of research carried out at the Jet Propulsion Laboratory, California Institute of Technology under Contract NAS7-100, sponsored by NASA. The authors wish to acknowledge many valuable interactions with J. Cole of UCLA and E. Murman of the NASA Ames Research Center during the course of this research. Their contributions to this work have been both timely and numerous. The authors wish to acknowledge the excellent assistance of C. Nussey and R. Morrow, and of the entire JPL wind tunnel staff in the performance of the experiments.

Index category: Subsonic and Transonic Flow.

* Senior Scientist, Physics Section. Member AIAA.

† Consultant; also Assistant Professor, Department of Mathematics, UCLA; present address; Director of Academic Computation, Middlebury College, Middlebury, Vt.

II. Experimental Technique

The experiments were performed in the Jet Propulsion Lab. 20-in. wind tunnel at Mach numbers $0.6 \leqq M_\infty \leqq 0.915$, and Reynolds numbers $1.2 \times 10^6 \leqq Re \leqq 3.6 \times 10^6$, based on chord. The 20-in. tunnel, shown in Fig. 1, is a continuous operating, variable density facility which has solid walls and a test section measuring 45.7 cm wide by 50.8 cm high. The present experiments were performed for a total pressure $P_o = 100$ cm Hg. For this condition, a high quality transonic flow is obtained by adjusting the walls such that the tunnel empty Mach number is constant throughout the entire region of interest. The Mach number is adjusted by use of a downstream throat, which provides steady, reproducible measurements.

The four circular-arc bodies employed in these experiments were constructed such that the geometrical transonic tunnel parameter

$$T = (H/c)\delta^{1/3} = 2.68 \tag{1}$$

remained constant, thus allowing the comparison of the scaled results given in Sec. IV. In constructing these models, no attempt has been made to include the Mach number function in the usual transonic tunnel parameter (cf. Sec. III), given by

$$\tilde{T} = M_\infty{}^{2/3}(H/c)\delta^{1/3} \tag{2}$$

The consequence of this omission will be discussed in Sec. IV. Two of the models were biconvex airfoils which were mounted in the center of the tunnel as shown in Fig. 1. These models, a 6% thick ($\delta = 0.0606$), 7.5 cm chord, and a 12% thick ($\delta = 0.1181$), 9.45 cm chord airfoil were formed by casting an epoxy aerodynamic surface over an instrumented center spar as described by Collins.[11] Mounted in the surface of each model are 27 static pressure taps arranged in six rows, three rows on each side of the model surface. Two of these taps, located at the 50% chord point on opposite sides of the model, were connected to a silicone oil U-tube manometer in order to set the angle of attack to zero. The entire lower surface of the airfoil was visible in order to provide both schlieren and shadowgraph information about the flowfield (cf. Fig. 1). The second series of bodies consisting of both a 12% thick ($\delta = 0.1187$) and a 20% thick ($\delta = 0.2068$) half-body, mounted on the wind-tunnel ceiling, were formed by an epoxy-filled metal skin, instrumented with static pressure taps. For these bodies, the entire flowfield was visible through 68-cm-diam windows, which were used to obtain schlieren photographs of the flow. In each case, the bodies spanned the 45.7 cm tunnel width.

Static pressure measurements on the tunnel floor and ceiling were obtained both by using existing orifices, and by the installation of a special rake visible on the ceiling in Fig. 1. This rake consists of twenty-one 1.04-mm-diam hypodermic tubes bonded to the tunnel, each containing an orifice at a different location. Simultaneous measurements of the pressure obtained from this rake and from adjacent orifices indicate excellent agreement. The measured boundary-layer thickness was approximately 2 cm; hence the rake causes no measurable disturbance to the freestream flow. All pressures were monitored using the JPL multiport measuring system and were recorded on the data acquisition system. The data system simultaneously records data from the stagnation pressure transducer and the freestream static pressure transducer, as well as from two 0–15 psia Statham pressure transducers, each of which sequentially samples 50 orifices through the MPMS. The combined accuracy of these measurements provides a Mach number resolution of 0.002 for a total pressure of 100 cm Hg.

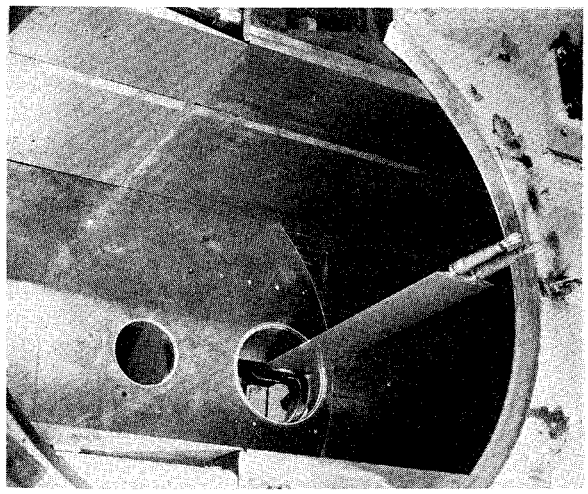

Fig. 1 12% thick biconvex airfoil mounted in the JPL 20-in. wind tunnel. Flow from the right.

III. Theoretical Method

In the present analysis, using singular perturbation methods, the full potential equation

$$(a^2-\Phi_x{}^2)\Phi_{xx}-2\Phi_x\Phi_y\Phi_{xy}+(a^2-\Phi_y{}^2)\Phi_{yy}=0$$
$$a^2 = a_\infty{}^2 - \frac{\gamma+1}{2}[U_\infty{}^2-\Phi_x{}^2-\Phi_y{}^2] \tag{3}$$

may be approximated by an expansion of the form (cf. Murman and Cole[4])

$$\Phi(x, y) = U_\infty\{x+f(M_\infty, \delta)\phi(x, \tilde{y})+\cdots\}$$

where

$$\tilde{y} = g(M_\infty, \delta)y \tag{4}$$

Substituting this expansion into Eq. (3), one obtains

$$g(M_\infty, \delta) = M_\infty\{f(M_\infty, \delta)\}^{1/2}$$

and hence

$$\tilde{y} = M_\infty\{f(M_\infty, \delta)\}^{1/2}y$$

and

$$\{K-(\gamma+1)\phi_x\}\phi_{xx}+\phi_{\tilde{y}\tilde{y}}=0$$

if

$$K = (1-M_\infty{}^2)/M_\infty{}^2 f(M_\infty, \delta) \tag{5}$$

Using a consistent expansion for the scaled pressure coefficient, $\bar{C}_p$ becomes

$$\bar{C}_p(x, \tilde{y}; K) = -2\phi_x(x, \tilde{y}; K) = C_p(x, \tilde{y})/f(M_\infty, \delta) \tag{6}$$

In a similar way, the boundary condition of tangent flow over affine bodies $\tilde{y} = (\delta/2)F(x)$ yields the form

$$\phi_{\tilde{y}}(x, \tilde{y}; K) = \tfrac{1}{2}d\{F(x)\}/dx \tag{7}$$

when

$$f(M_\infty, \delta) = (\delta^{2/3}/M_\infty{}^{2/3})$$

and hence

$$K = (1-M_\infty{}^2)/M_\infty{}^{4/3}\delta^{2/3} \tag{8}$$

as given by Spreiter.[1] Under these conditions, Eq. (6) yields a scaled pressure coefficient given by

$$\bar{C}_p(x, \tilde{y}) = (M_\infty{}^{2/3}/\delta^{2/3})C_p(x, \tilde{y}) \tag{9}$$

and Eq. (5) yields a transonic tunnel height parameter based on the scaled wall coordinate

$$\tilde{T} = M_\infty{}^{2/3}(H/c)\delta^{1/3} \tag{10}$$

where H is defined as twice the distance from the plane of symmetry of the model to the tunnel wall. Therefore H is equal to the tunnel height (50.8 cm) for the biconvex airfoils.

For a symmetric body, $y_\pm = \pm(\delta/2)F(x)$, $|x| \leqq \frac{1}{2}$, aligned with the flow, the resulting boundary value problem becomes

$$\{K-(\gamma+1)\phi_x\}\phi_{xx}+\phi_{\tilde{y}\tilde{y}}=0 \tag{11}$$

$$\phi_{\tilde{y}}(x, 0) = \begin{cases} \frac{1}{2}F'(x) & |x| < \frac{1}{2} \\ 0 & |x| > \frac{1}{2} \end{cases} \tag{12}$$

$$\phi_{\tilde{y}}(x, \tilde{T}) = 0 \quad \text{(solid-wall wind tunnel)}$$
$$\phi_x \to 0 \quad \text{as} \quad |x| \to \infty$$

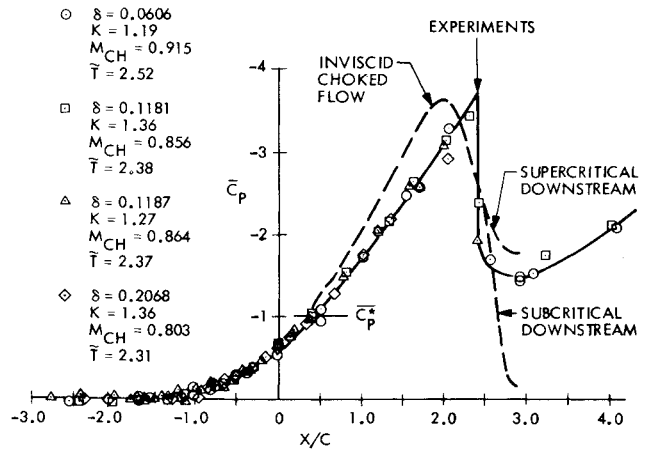

Fig. 2 Pressure distribution on the wind-tunnel wall using the Spreiter scaling for the pressure coefficient. Choked flow, $K = 1.36$.

Symmetry is used to solve the problem only for $\tilde{y} \geqq 0$. Following the procedure of Murman and Cole,[4] an asymptotic formula for ϕ as $|x| \to \infty$ has been derived in the form

$$\phi \sim \pm \frac{\mathscr{D}}{K\tilde{T}} + 0\left(e^{\frac{-2\pi|x|}{\tilde{T}K^{1/2}}}\right) \quad \text{as} \quad x \to \pm\infty \tag{13}$$

where

$$\mathscr{D} = 2\int_{-1/2}^{t/2} F(\xi)\,d\xi + (\gamma+1)\int_0^{\tilde{T}}\int_{-\infty}^{\infty} \phi_{\tilde{\xi}}{}^2\,d\xi\,d\tilde{y} \tag{14}$$

Equation (11), subject to the boundary conditions given in Eqs. (12) and (13), has been solved by the relaxation method first described by Murman and Cole.[4] For most of the computations presented here, the computational mesh consisted of 90 points in the x-direction ($-2.0 \leqq x \leqq 3.5$), and 37 points in $\tilde{y}$. For this mesh it was found that the second term in Eq. (13) was exponentially small, and it has not been used in the solutions presented.

For all values of $K > K_{ch}$, where K_{ch} is the value of K at which the sonic line first reaches the wall, $\tilde{y} = \tilde{T}$, the use of the boundary conditions given in Eqs. (12) and (13) together with Eq. (11) lead to solutions which converged rapidly and exhibit excellent agreement with experimental data. Attempts to lower K below K_{ch}, and to retain the boundary conditions specified in Eqs. (12) and (13), lead to solutions which failed to converge. This is consistent with our physical concept of choked flow. At choking, the upstream flowfield becomes independent of the downstream flow, and hence the upstream Mach number, or K, is no longer allowed to change with decreasing downstream pressure. Therefore, once $K = K_{ch}$, the boundary conditions given in Eqs. (12) and (13) were replaced by $\phi = \text{const}$ upstream and a prescription of ϕ_x (pressure) downstream. This prescription of the boundary conditions resulted in a fully converged solution which is completely supersonic downstream. This point will be discussed further in Sec. IV.

It is important to note that it was necessary to use the fully conservative differencing scheme recently developed by Murman[6] in order to obtain a fully converged solution for the flow near choking. This was necessary because the difference scheme previously given by Murman and Cole[4] gave an erroneous description of the flowfield away from the body whenever a substantial supersonic zone was present.

IV. Experimental and Theoretical Results

A. Transonic Scaling

If we consider the derivation of Eq. (11) in the previous section in terms of a limit process such that K remains fixed as $\delta \to 0$ and $M_\infty \to 1$, then M_∞ can be replaced by unity in Eqs. (9) and (10), and in the denominator in Eq. (8). In an attempt to extend the range of validity of Eq. (11), many different scaling laws have been suggested (cf. Krupp[5] and Murman and Cole[4]). The test of the validity of any one of these laws must be its ability to scale the experimental data for Mach numbers substantially different from unity.

Experimental evidence has been given previously for the validity of scaling in the vicinity of $M_\infty = 1.0$. Spreiter,[12] using the data of Drougge,[13] has demonstrated the validity of these ideas by scaling data from axisymmetric bodies of differing thickness (cf. Ferrari and Tricomi[14]). For two-dimensional flows, Michel et al.[15] have also demonstrated the correspondence of the pressure distribution obtained at $M_\infty = 1.0$ from four circular-arc models. However, these results do not include data for upstream Mach numbers substantially different from unity. Figure 2 shows the results of the pressure distribution generated on the solid wall of the wind tunnel by the four models described in Sec. II under conditions for which the flow is choked. In this figure, $\bar{C}_p$ is defined by Eq. (9), corresponding to the formulation by Spreiter. The corresponding values of both the choked Mach number, and of the transonic scaling parameter K, given by Eq. (8), are listed for each case, together with the thickness ratio δ and the tunnel parameter $\tilde{T}$. Included in this figure are results of the inviscid computations for the choked flow over the 6% biconvex model. The agreement exhibited between theory and experiment in this case will be discussed in detail in the next section.

Figure 3 shows the results obtained from both the 6% and the 12% thick biconvex airfoils mounted in the center of the tunnel. The data from the choked case, corresponding to the data shown in Fig. 2, are shown in the upper portion of the figure, together with the results computed from inviscid theory. The agreement between the theory and the experiments is well within the 3% difference between the two experimental cases shown. This figure, together with Fig. 2, confirms the ideas of scaling for Mach

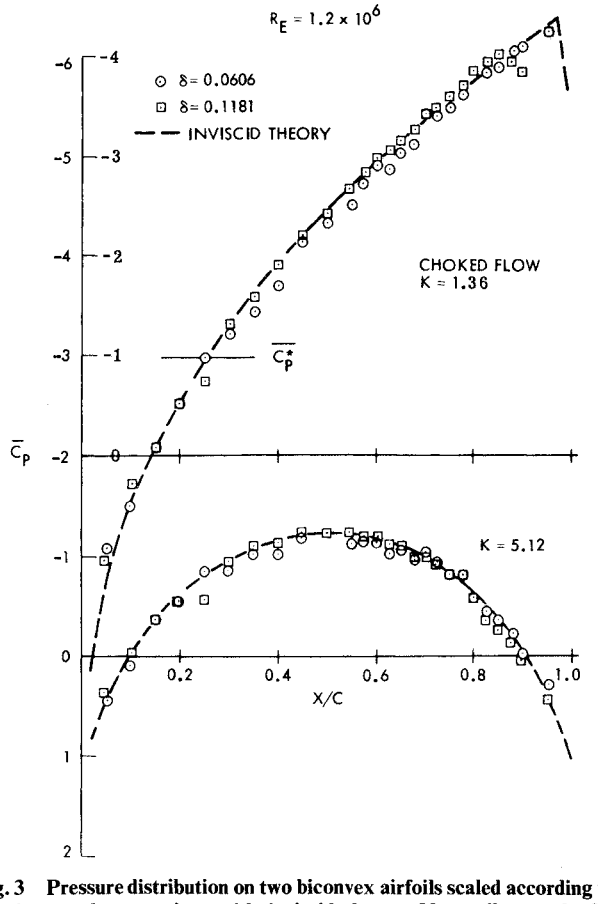

Fig. 3 Pressure distribution on two biconvex airfoils scaled according to Spreiter, and comparison with inviscid theory. Note offset scale for $K = 1.36$.

numbers near unity. The flow near choking will be considered in detail in the next section.

The results presented in the lower portion of Fig. 3 for the same two airfoils ($K = 5.1$) correspond to a completely subcritical case ($K_{crit} = 2.58$), and represent data for which the free-stream Mach number differs greatly from unity. The corresponding wall pressure distribution measrements for this case exhibit negligible perturbation from uniform flow, and consequently are not shown here. These results demonstrate the validity of the inviscid scaling laws given by Eqs. (8) and (10) for flows whose Mach numbers are considerably below one.

For the Reynolds numbers of these experiments, the pressure distributions generated by the wall mounted bodies (cf. Sec. II) are influenced by the approach boundary layer and have not been included in Fig. 3. The present experiments indicate that the interaction with the approaching boundary layer is confined to a region near the leading and trailing edge of the model whose extent is of the order of the thickness of the approach boundary layer, as predicted by Cole.[16] The pressure distribution which results from this interaction scales according to the rules outlined in Sec. III. The results given in Fig. 2, on the other hand, confirm Guderley's[7] predictions that the far field generated by this interaction does not differ measurably from that generated by the biconvex models. A more detailed discussion of the independence of the wall pressure distribution of the details of the flow near the body will be given in the next section.

The data presented in Figs. 2 and 3, together with the results from inviscid theory for the same conditions, demonstrate the validity of the scaling laws given in Eqs. (8) and (10) for affine bodies whose thickness ratio is nonvanishing, and for Mach numbers that differ substantially from unity. This is not to imply that the scaling is unique, however. The scaling given by Krupp[5] yields a disparity of only 7% at the midchord station for this large value of K, compared to the 3% discrepancy of the data shown in Fig. 3. However, it has been found that, even for Mach numbers near the critical value, substantial differences arise when the limiting form suggested by Murman and Cole[4] is used to scale the present experiments. The validity of a particular form of the transonic scaling parameter cannot be determined with more precision using circular-arc bodies, but must be obtained from bodies whose pressure distributions show more pronounced behavior near the leading edge (cf. Krupp[5]).

B. The Flow Near Choking

The phenomena associated with the choking of a solid-wall wind tunnel are of interest because of their importance in defining a limiting case of wind-tunnel wall interference, and because of the representation thus afforded of the unbounded flow near $M_\infty = 1.0$.

Figure 4 is a composite sketch of the development of the flow over a 20% thick half-body, mounted on the wind-tunnel ceiling,

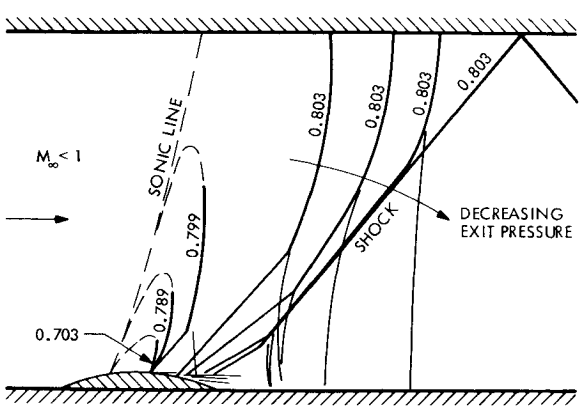

Fig. 4 The flow pattern near choking for a 20% wall mounted body. $Re = 3.6 \times 10^6$, $M_{crit} = 0.669$, $M_{ch} = 0.803$. Note the pattern inversion created by schlieren photography.

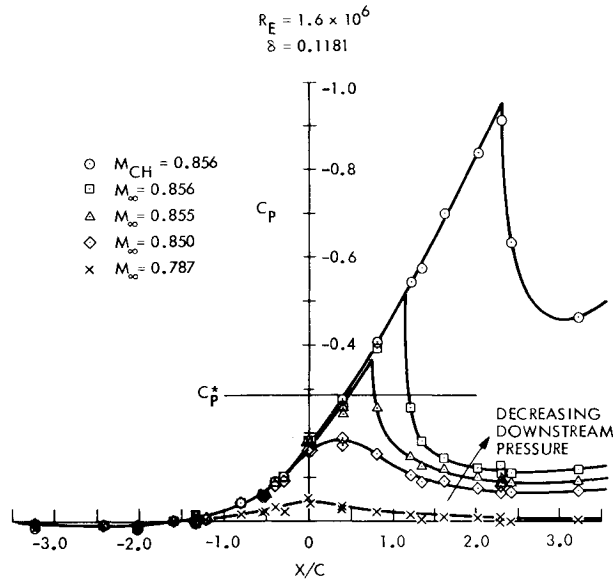

Fig. 5 Pressure distribution on the wind-tunnel wall for the 12% thick biconvex airfoil near choking.

as the Mach number is increased from its critical value ($M_{crit} = 0.669$) to that corresponding to choked flow ($M_{ch} = 0.803$) by decreasing the downstream pressure. The data were obtained by tracing the flow patterns from a succession of schlieren photographs, which accounts for the apparent inversion of the model position suggested in Fig. 4. The location of the sonic line indicated in the figure has been represented from measurements of the location of its end points, available from pressure measurements on the body and on the tunnel wall, and should not be assumed to be precise.

As the Mach number for the flow illustrated in Fig. 4 is increased beyond the critical value to approximately $M_\infty = 0.78$, the sonic zone grows slowly and both the peak Mach number on the body and the peak Mach number on the wall are nearly proportional to M_∞ (cf. Fig. 7). Beyond this Mach number, the flow both over the model and adjacent to the opposite wall accelerates rapidly with increasing Mach number. As the downstream pressure is decreased further, the sonic line intercepts the opposite wall, isolating the flow upstream of the sonic line from any further changes in the downstream boundary condition. This condition, that the sonic line intercepts the opposite wall, establishes the Mach number, and hence the value of K at which choking occurs. As the downstream pressure is reduced further, the region of supersonic flow between the sonic line and the shock wave increases in extent as illustrated in Fig. 4. So long as the flow downstream of the shock is subsonic at any point along its length, the shock location, and hence the flow pattern, depends on the downstream pressure. Thus an entire family of flows is generated for which the upstream Mach number is constant and equal to the choked Mach number. In each case, the flow upstream of the shock wave is independent of the downstream pressure, and only the shock wave location is permitted to vary, as illustrated in Fig. 5. As the downstream pressure is decreased further, the shock wave becomes oblique over its entire length, and the flow downstream of the shock becomes entirely supersonic. This condition represents a second limit in the choking process. Any further decrease in the downstream pressure has no influence on the flow pattern under consideration.

The flow patterns given in Fig. 4 are both stable and reproducible, and represent a family of flows which depend on the downstream boundary conditions much as the flow in a choked nozzle depends on the back pressure.

The data shown in Fig. 5 illustrates the behavior of the flow adjacent to the wind-tunnel wall for conditions near choking. Upstream of the leading edge station ($x/c = -0.5$), the pressure

distribution is independent of the final flow state except at the lowest Mach number. Between $M_\infty = 0.850$, for which the shock wave runs approximately one-half of the way across the tunnel for the case of the 12% biconvex airfoil, and $M_\infty = 0.855$, for which choking occurs, the flow accelerates and becomes sonic at the wall. The flow downstream of the shock continues to be subsonic, however. As the downstream pressure is reduced further, the flow accelerates over the rear of the model, and an oblique shock forms on the tail, leaving an extensive zone of supersonic flow downstream of the body. The 12% biconvex airfoil data has been chosen for Fig. 5, rather than the data corresponding to Fig. 4, because of the greater extent of pressure data available downstream for the airfoil. The scaling demonstrated in Fig. 2 and discussed at length in the previous section permits an extension of the results presented in Fig. 5 to the other cases under consideration.

An alternative way of viewing the wind-tunnel wall pressure distribution for choked flow is illustrated by the results shown in Fig. 6, where the data is again plotted in scaled coordinates. Spreiter et al[9] have shown that for flows near $M_\infty = 1.0$, the classical scaling relations, derived for small perturbations from sonic speed, yield an expression for the choked Mach number in terms of a body shape function A, given by

$$(1-M_{ch})(T^{2/5}/\delta^{2/3}) = A \tag{15}$$

From experiments, Spreiter et al.[9] have shown that for a double-wedge airfoil

$$(1-M_{ch})(T^{2/5}/\delta^{2/3}) = A = 1.127$$

For the circular-arc profile, the present experiments give the value

$$(1-M_{ch})(T^{2/5}/\delta^{2/3}) = A = 0.84$$

According to the theory of Guderley,[7,17] the choked flow near the wall is independent of the body shape function when plotted in terms of the coordinate system used in Fig. 6

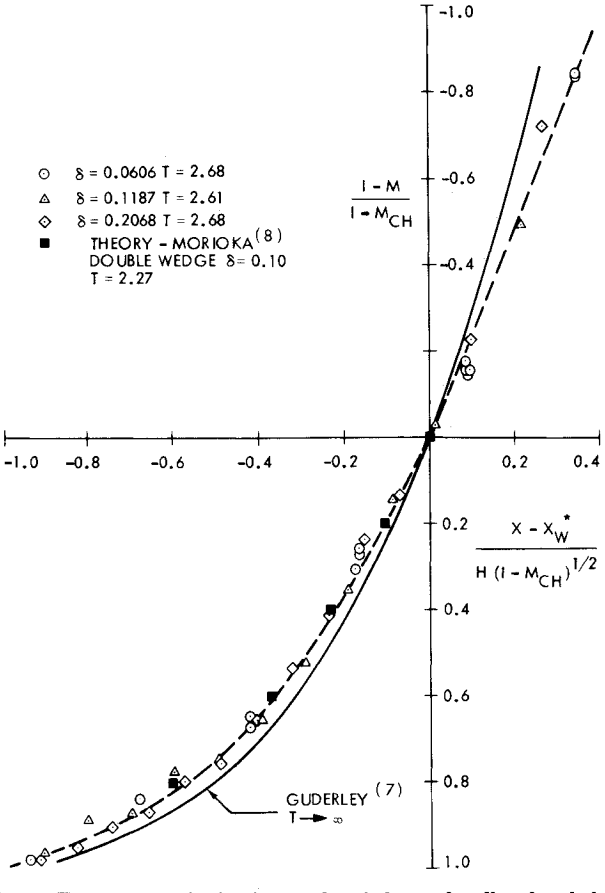

Fig. 6 The pressure distribution on the wind-tunnel wall under choked flow conditions using the Guderley scaling.

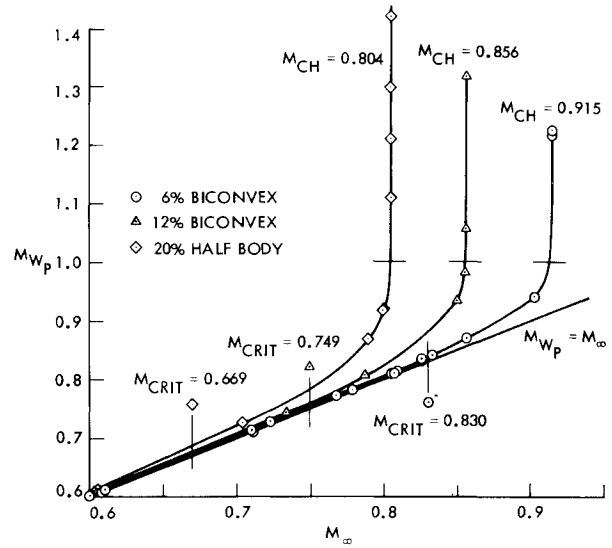

Fig. 7 The peak wall Mach number as a function of the freestream Mach number for a solid-wall wind tunnel. Data from a 6% and a 12% biconvex airfoil and a 20% half body.

$$\frac{1-M}{1-M_{ch}} \sim \frac{T^{2/5}}{A}\bar{C}_p \frac{x-x_w^*}{H(1-M_{ch})^{1/2}} \sim \frac{x/c}{T^{4/5}A^{1/2}} \tag{16}$$

which contains both the profile shape function A and the geometrical tunnel parameter T. The solid line in Fig. 6 represents the Guderley[7] theory for the limit of a large tunnel parameter, $T \to \infty$. Compared to the theory by Guderley are the theoretical results given by Morioka[8] for a double-wedge airfoil with $T = 2.27$, represented by the solid squares in the figure, and the present experimental data ($T = 2.68$) for the three circular-arc airfoils listed in the figure. The dashed curve is used to fit the data. These results again verify the inviscid scaling laws for the particular case of choked flow, and in addition demonstrate the independence of the scaling from the body shape parameter as discussed previously, and the dependence on the tunnel parameter.

The extreme sensitivity of the flow to the freestream Mach number in the vicinity of choking as illustrated in Fig. 5 is characteristic of these flows. This sensitivity is demonstrated by the approach to the choked condition shown in Fig. 7, where the peak Mach number on the tunnel wall is plotted as a function of the freestream Mach number for both the 6% and the 12% biconvex airfoils and for the 20% half body. These data show that the peak wall Mach number increases linearly with M_∞ up to the critical Mach number. For supercritical flows, the flow near the wall is rapidly accelerated and becomes sonic at the Mach number corresponding to choking. At this Mach number, the slope is infinite and the peak wall Mach number becomes independent of the freestream Mach number and depends only on the downstream pressure (cf. Figs. 4 and 5).

A more graphic representation of the behavior of the flow near choking is shown in Fig. 8 where the peak wall pressure coefficient given by Eq. (9) is shown as a function of the transonic scaling parameter K given by Eq. (8). The use of the Spreiter scaled coordinates serves to collapse the data given in Fig. 7 into a single curve in agreement with the theoretical predictions, shown as the solid symbols in the figure. This figure shows that in the vicinity of choking the data for both the 6% airfoil and for the theory differ somewhat from the remainder of the data shown in Fig. 8. The cause of the disagreement for the 6% airfoil data is believed to lie in the somewhat larger tunnel parameter used in this case ($\tilde{T} = 2.52$ as compared to 2.38 for the 12% airfoil, cf. Fig. 2). This fact results in a lower value for K for choked flow. The difference exhibited by the theory will be discussed in subsequent paragraphs.

The sensitivity near choking is duplicated in the theoretical calculations, presented in Figs. 2 and 3 for the choked flow

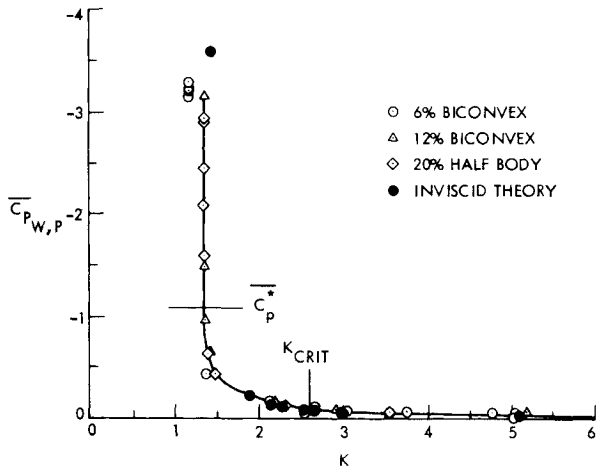

Fig. 8 The peak wall pressure coefficient, scaled after Spreiter, as a function of the transonic scaling parameter K.

over the 6% biconvex airfoil and in Fig. 8. These calculations demonstrate the importance of prescribing the proper boundary conditions for computations of the choked flow case. The flows illustrated in Figs. 2 and 3 were computed by prescribing the normal asymmetric boundary conditions [cf. Eq. (12)] on the potential for $K \geqq 1.5$ ($M_\infty = 0.89$). For $K < 1.5$, logic was introduced to permit switching of the boundary conditions according to whether or not the sonic line reached the opposite wall. When the flow at the wall reached sonic velocity, the upstream boundary condition was no longer allowed to vary, and the downstream boundary condition was changed to a prescription of ϕ_x, which is equivalent to a prescription of the downstream pressure as in the experiments. Two choked flow solutions have been computed for $K = 1.49$ ($\delta = 0.0606$; $\tilde{T} = 2.68$), which correspond to the two branches of the inviscid curve shown in Fig. 2. The first was computed for $\phi_x = 0.025$ downstream and exhibits a subcritical flow beyond the shock wave. For the second case, ϕ_x was increased until the solution was entirely supersonic on the downstream boundary. This procedure for ϕ_x is entirely consistent with the experiments, in which the downstream pressure is lowered to achieve a fully choked flow.

The excellent agreement achieved in the latter case for the flow over the 6% airfoil is shown in Fig. 3. The agreement between the computed pressure distribution at the wall and the experiments (cf. Fig. 2) is not as good, but clearly demonstrates the proper behavior. For the flow near the wall, the deviation between theory and experiment originates upstream of the sonic line and results in a peak value of C_p which occurs upstream of the shock wave. However, the location for the oblique shock wave, based on a maximum slope criterion, is nearly identical to the experiments. The experiments indicate a well defined shock wave, while the theory indicates a compression that is spread over several mesh points with a sizable influence.

The major disagreement between theory and experiment, however, is in the prescribed value of K necessary to achieve choked flow ($K_{\text{theory}} = 1.49$; $K_{\text{exp}} = 1.19$ for $\delta = 0.0606$, $\tilde{T} = 2.52$). For $\tilde{T} = 2.38$, the value of the scaling parameter for which choking occurs in the experiments ($K = 1.36$) has been obtained from the results shown in Figs. 2 and 8. The maximum deviation from this value occurs for the case of the 6% airfoil ($K = 1.19$; cf. Fig. 8) and results as a consequence of the failure to account for the Mach number dependence of the transonic tunnel parameter $\tilde{T}$ in the construction of the models. This point is only important for flows near choking, for which the wall is near the body in the transonic sense. The value obtained for K from the theory ($K = 1.49$) corresponds to a choked Mach number $M_{ch} = 0.898$ for the 6% airfoil, relative to a measured choked Mach number $M_{ch} = 0.915$, and equals the Mach number ($M = 0.899$) obtained from a standard one-dimensional calculation.

We do not at this time have an adequate explanation of the difference between the choking Mach number M_{ch} from theory and experiment. Several factors may contribute to the differences between theory and experiment. The first possibility is that viscous effects, which are excluded in the theory, are influential in the experiments. For the present experiments the interaction between the shock wave and the wind-tunnel boundary layer is not sufficiently strong to cause separation. However, this interaction will increase the boundary-layer thickness and produce an effective decrease in the tunnel parameter, and hence an increase in K at choking, in opposition to the observed effect. At the model a somewhat different picture emerges. For the biconvex models, the Reynolds numbers are sufficiently high that the model boundary layer is fully turbulent over a substantial portion of the model. The pressure gradient induced by the shock wave at the trailing edge is insufficient to cause separation on either of the biconvex models. As a consequence, the wake is thin and although its influence is to reduce the effective model thickness, and hence decrease the value of K at choking as observed, the effect should be small and should play little role in the modification of the downstream boundary condition specified for the inviscid computations. For the ceiling mounted bodies (cf. Fig. 4), the interaction is more complex. Separation of the turbulent boundary layer by the shock wave generates the lambda character of the shock wave near the body, with separation occurring near the forward intersection shown in Fig. 4. This case is analogous to the flow discussed by Alber et al.[18] as Case B. A partial description of the separation process is given in Ref. 19.

The computations of the flow over the 6% airfoil most probably disagree with the experiments as a result of the inadequate choice of the boundary conditions at the upstream and downstream boundaries. The modifications of these boundary conditions may require viscous corrections as well as a more accurate description of the inviscid flowfield. However, because of the observation that near choking the pressure distribution on the airfoil experiences a Mach number independence that is analogous to the sonic freeze phenomenon observed for unbounded flows, it is unlikely that the modifications necessary to effect the small change in K_{ch} required for agreement with the proper experimental value would have any substantial effect on the agreement between theory and experiment on the airfoil.

For a particular airfoil, a close analogy exists between choked flow in a solid-wall tunnel and unbounded flow at $M_\infty = 1.0$

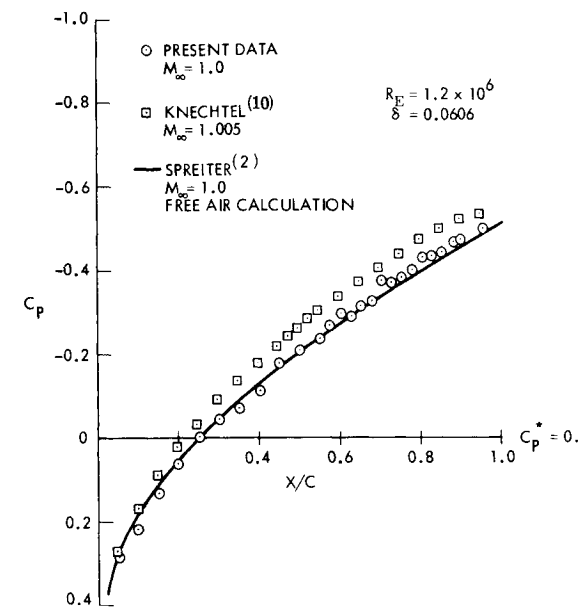

Fig. 9 Comparison of the pressure distribution on a 6% biconvex airfoil at sonic speed. Present data for choked flow computed by assuming $M_\infty = 1.0$.

because of the existence of a limiting characteristic for sonic unbounded flow which is asymptotic to the sonic line at infinity, and consequently isolates the flowfield upstream of this characteristic from the behavior downstream. By analogy, when the sonic line reaches the wall for the choked case, a new limiting characteristic is introduced upstream of the location defined for the unbounded flow. This characteristic is that which reaches the sonic line at the wall. Characteristics upstream of the limiting choked flow characteristic, which contain expansion information from the body, reflect as compression characteristics from the sonic line. Downstream of this characteristc, expansion waves reflect from the solid wall as expansion waves, modified of course by the wall boundary layer. The consequence of these facts is that the flowfield upstream of the choked flow limiting characteristic will be representative of that appropriate to sonic unbounded flow. If the analogous flow in the tunnel is fully choked, the flow between the limiting characteristic and the shock will also be representative of the unbounded sonic flow, modified by the second-order effects introduced by the expansion waves reflected from the wall.

A test of this analogy between choked flow and the unbounded flow at $M_\infty = 1.0$ is illustrated in Fig. 9 for the pressure distribution on an airfoil. In this figure, data from the 6% biconvex airfoil under choked flow conditions have been reduced by stating that $M_\infty = 1.0$, and computing C_p accordingly. These results are plotted in Fig. 9 as a function of chordwise position, and are compared with the theoretical results of Spreiter and Alksne[2] for unbounded flow at $M_\infty = 1.0$. The Spreiter and Alksne results have recently been reproduced at Mach numbers slightly in excess of one by Murman[20] and are believed to be an accurate representation of the unbounded sonic freestream flow. The agreement between the choked flow results and the unbounded flow theory is excellent. For $x/c > 0.65$, a noticeable trend appears in the data which may be a consequence of the finite tunnel parameter; however, the maximum value of this discrepancy does not exceed about 4%. In contrast, the experimental data of Knechtel,[10] obtained in a porous-wall tunnel at $M_\infty = 1.0$, shows significant disagreement over the entire chord. The reasons for this difference may lie in the fact that a porous tunnel at $M_\infty = 1.0$ allows communication between the downstream and the upstream flows through the plenum chamber used to cancel the reflected waves. Thus the duplication of the sonic result of an isolated upstream flow is not achieved. Knechtel's results for a solid-wall tunnel operating at the choked condition have not been shown in Fig. 9. These results lie between the data from the current experiments and that for the porous-wall facility.

C. Comparison of Experimental Results

A summary of the pressure distribution measurements for the 6% thick biconvex airfoil at a Reynolds number $Re = 1.2 \times 10^6$ is compared in Fig. 10 with the results of the theoretical calculations outlined in Sec. III, and with corresponding measurements by Knechtel[10] obtained in a porous-wall wind tunnel at $Re = 2.0 \times 10^6$. These results indicate that for $M_\infty < M_{\text{crit}}$, excellent agreement exists between the present results and those of Knechtel. For $M_\infty = 0.857$, the first supercritical case presented, a difference appears between the present data and that of Knechtel near the region of minimum pressure coefficient, and in the vicinity of the shock. Further increases in Mach number to $M_\infty = 0.903$, $M_{ch} = 0.915$ also exhibit differences in the vicinity of the shock wave. This behavior is consistent with the wall interference exhibited in Figs. 7 and 8 which delays the shock wave formation, and has the net effect of producing a flowfield which is appropriate to a higher freestream Mach number. These differences arise because of the different boundary conditions which exist in the two experiments and are supported by the computations of Murman.[21]

The comparisons shown in Fig. 10 between the present experiments and inviscid theory are exact for $M_\infty < M_{\text{crit}}$. For $M_\infty = 0.857$, a 5% discrepancy immediately preceding the shock wave is thought to be the consequence of viscous effects as both the shock wave location and the pressure distribution on either

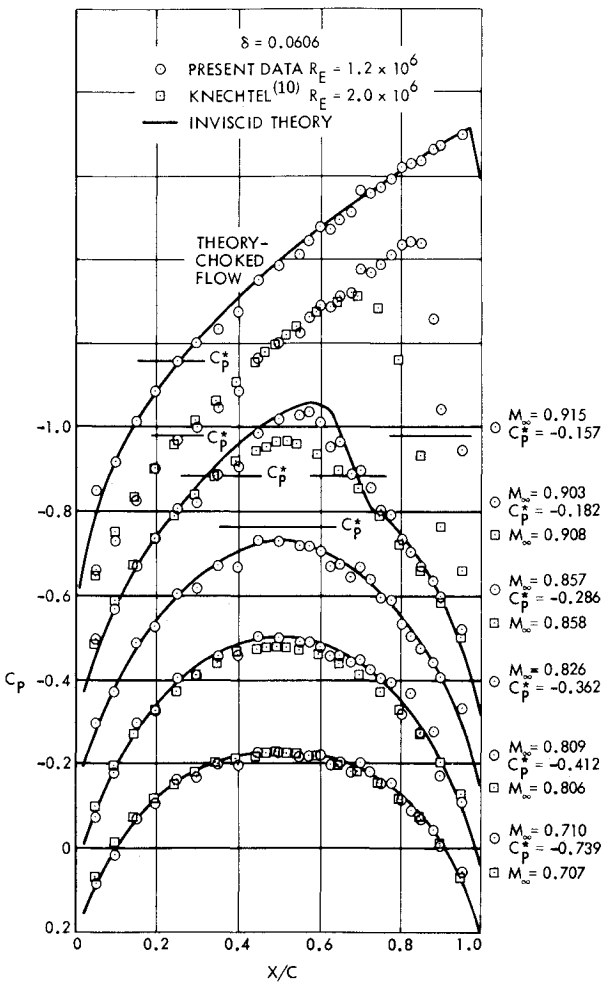

Fig. 10 Pressure distribution on the 6% biconvex airfoil as a function of Mach number for $Re = 1.2 \times 10^6$. Present data compared with that of Knechtel[10] and with inviscid theory. Note offset scales.

side of the shock wave show exact agreement. No computation has been made for the $M_\infty = 0.903$ data shown in Fig. 10. As stated in the previous section, the choked flow solution shows good agreement with experiment when the computation corresponding to a supercritical downstream boundary condition is used, even though the computed Mach number is in error.

The question of a possible relationship between the flowfield measured in a solid-wall wind tunnel and that obtained from the same body in a porous-wall wind tunnel has led to the *empirical* observation that excellent correspondence can be obtained between the present measurements and those of Knechtel[10] if the current data for supercritical flows (cf. Fig. 10) are reduced by using the measured peak wall Mach number given in Fig. 7 in place of the measured freestream Mach number when $M_{wp} \leqq 1.0$, and by using unity for choked flows. As shown in Fig. 9, this criterion, when applied to choked flow, yields the results for an unbounded flow at $M_\infty = 1.0$, and not the porous wall result. For Mach numbers below unity, however, the porous tunnel is expected to yield results that are representative of unbounded flows. It must be emphasized, however, that this is an *empirical* result and has no basis in theory.

Correlations of the present data with that of Liepmann, Ashkenas, and Cole,[22] and of Liepmann[23] have not been successful. Symptomatic of the problem is the fact that the critical Mach number reported by Liepmann[23] ($M_{\text{crit}} = 0.899$) is considerably higher than that observed either in the present results or by Knechtel.[10] This is perhaps a consequence of the aspect ratio ($\mathcal{A}\mathcal{R} = \frac{2}{3}$) used in the early experiments, but is more likely a consequence of an observed freestream Mach number gradient that has been noted in those measurements.

The experiments of Michel et al.[15] have also been examined. The result for the critical Mach number for the 6% half-body ($M_{crit} = 0.875$) reported in Ref. 15 does not correspond to the present result, which may be a consequence of the effect of the approach boundary layer on the pressure distribution on a model mounted on the tunnel floor.

The data obtained by Wood and Gooderum[24] for the pressure distribution on a 12% thick biconvex airfoil in a freejet agrees with the present data over the forward portion of the model, up to the midchord position. In addition, the measured values of the critical Mach number are in exact agreement for the two experiments. However, the measured pressure distributions do not agree in the region downstream of the shock wave. For example, Wood and Gooderum report that for $M_\infty = 0.861$, $C_{p\,max} = -0.60$ at $x/c = 0.5$, and subsequently the flow separates, whereas the present results for $M_{ch} = 0.856$ exhibit fully attached flow (cf. Fig. 3).

V. Conclusions

A combined experimental and theoretical program has been described in which the flows generated by a family of transonically scaled circular-arc bodies mounted in a solid-wall wind tunnel have been studied for Reynolds numbers $1.2 \times 10^6 \leqq Re \leqq 3.6 \times 10^6$, and for Mach numbers $0.6 \leqq M_\infty \leqq 0.915$. The results for this investigation have shown that for $Re \geqq 10^6$, for which the turbulent boundary layer is thin and remains attached, inviscid theory gives an excellent representation of the flowfield over the body. Near choking in the solid-wall facility, the computations yield a reasonable description of the flowfield, but do not reproduce the proper choked Mach number or the pressure distribution on the wall. The flowfields at high Reynolds number are shown to be similar when scaled with the transonic scaling laws given by Spreiter,[1] and the choked flow experiments show excellent agreement with the approximate theories of Guderley[7] and Morioka[8] for the choked flow over a thin airfoil. The experiments have been used to provide a detailed description of the phenomenon of choking in a solid-wall wind tunnel, and an analogy has been discussed which relates the results for choked flow to the flow at $M_\infty = 1.0$ over an airfoil in an unbounded stream.

References

[1] Spreiter, J. R., "On the Application of Transonic Similarity Rules to Wings of Finite Span," Rept. 1153, 1954, NACA.

[2] Spreiter, J. R. and Alksne, A. Y., "Thin Airfoil Theory Based on Approximate Solution of the Transonic Flow Equation," Rept. 1359, 1958, NACA.

[3] Cole, J. D., "Twenty Years of Transonic Flow," Rept. D1-82-0878, July 1969, The Boeing Co., Seattle, Wash.

[4] Murman, E. M. and Cole, J. D., "Calculation of Plane Steady Transonic Flows," *AIAA Journal*, Vol. 9, No. 1, Jan. 1971, pp. 114–121.

[5] Krupp, J. A., "The Numerical Calculation of Plane Steady Transonic Flows Past Thin Lifting Airfoils," Rept. D180-12958-1, June 1971, The Boeing Co., Seattle, Wash.

[6] Murman, E. M., "Analysis of Embedded Shock Waves Calculated by Relaxation Methods," AIAA Computational Fluid Dynamics Conference, Palm Springs, Calif., 1973.

[7] Guderley, G., "The Wall Pressure Distribution in a Choked Tunnel," TR 53-509, Dec. 1953, Wright Air Development Center, Wright-Patterson Air Force Base, Ohio.

[8] Morioka, S., "High Subsonic Flow Past a Wedge in a Two-Dimensional Wind Tunnel at its Choked State," *Journal of the Physical Society of Japan*, Vol. 14, No. 8, Aug. 1959, pp. 1098–1101.

[9] Spreiter, J. R., Smith, D. W., and Hyett, B. J., "A Study of the Simulation of Flow with Free-Stream Mach Number 1 in a Choked Wind Tunnel," TR R-73, 1960, NASA.

[10] Knechtel, E. D., "Experimental Investigation at Transonic Speeds of Pressure Distribution over Wedge and Circular-Arc Airfoil Sections and Evaluation of Perforated-Wall Interference," TN D-15; Aug. 1959, NASA.

[11] Collins, D. J., "An Inexpensive Technique for the Fabrication of Two-Dimensional Wind-Tunnel Models," *Review of Scientific Instruments*, Vol. 44, No. 7, July 1973, p. 855.

[12] Spreiter, J. R., "Aerodynamics of Wings and Bodies at Transonic Speeds," *Journal of the Aerospace Sciences*, Vol. 26, No. 8, Aug. 1959, pp. 465–486.

[13] Drougge, G., "An Experimental Investigation of the Interference Between Bodies of Revolution at Transonic Speeds with Special Reference to the Sonic and Supersonic Area Rules," Rept. 83, 1959, Aeronautical Research Institute of Sweden (FFA), Stockholm, Sweden.

[14] Ferrari, C. and Tricomi, F., *Transonic Aerodynamics*, Academic Press, New York, 1968, p. 609.

[15] Michel, R., Marchaud, F., and LeGallo, J., "Étude des Écoulements Transsoniques Autour des Profils Lenticulaires, A Incidence Nulle," TP 65, 1953, ONERA, France.

[16] Cole, J. D., private communication, Jan. 1972, Jet Propulsion Lab., Pasadena, Calif.

[17] Guderley, K. G., *The Theory of Transonic Flow*, Pergamon Press, London, 1962, pp. 274–280.

[18] Alber, I. E., Bacon, J. W., Masson, B. S., and Collins, D. J., "An Experimental Investigation of Turbulent Viscous-Inviscid Interactions," *AIAA Journal*, Vol. 11, No. 5, May 1973, pp. 620–627.

[19] Collins, D. J. and Krupp, J. A., "Experimental and Theoretical Investigations in Two-Dimensional Transonic Flow," AIAA Paper 73-659, Palm Springs, Calif., 1973.

[20] Murman, E. M., "A Relaxation Method for Calculating Transonic Flows with Detached Bow Shocks," Third International Conference on Numerical Methods in Fluid Dynamics, July 3–7, 1972, Paris, France.

[21] Murman, E. M., "Computation of Wall Effects in Ventilated Transonic Wind Tunnels," AIAA Paper 72-1007, Palo Alto, Calif., 1972.

[22] Liepmann, H. W., Ashkenas, H., and Cole, J. D., "Experiments in Transonic Flow," TR 5667, Feb. 1948, U.S. Air Force Air Material Command, Wright-Patterson Air Force Base, Ohio.

[23] Liepmann, H. W., "The Interaction Between Boundary Layer and Shock Waves in Transonic Flow," *Journal of the Aeronautical Sciences*, Vol. 13, No. 12, Dec. 1946, pp. 623–637.

[24] Wood, G. P. and Gooderum, P. B., "Investigation with an Interferometer of the Flow Around a Circular-Arc Profile at Mach Numbers Between 0.6 and 0.9," TN 2801, Oct. 1952, NACA.